PHYSICAL REVIEW B **95**, 205134 (2017)

Quantum oscillation studies of the topological semimetal candidate ZrGeM (M = S, Se, Te)

J. Hu,[1,*] Y. L. Zhu,[1] D. Graf,[2] Z. J. Tang,[1] J. Y. Liu,[1] and Z. Q. Mao[1,†]
[1]*Department of Physics and Engineering Physics, Tulane University, New Orleans, Louisiana 70118, USA*
[2]*National High Magnetic Field Lab, Tallahassee, Florida 32310, USA*

(Received 17 February 2017; published 22 May 2017)

The *WHM*-type materials (W = Zr/Hf/La, H = Si/Ge/Sn/Sb, M = O/S/Se/Te) have been predicted to be a large pool of topological materials. These materials allow for fine tuning of spin-orbit coupling, lattice constant, and structural dimensionality for various combinations of W, H, and M elements, thus providing an excellent platform to study how these parameters' tuning affects topological semimetal state. In this paper, we report high field quantum oscillation studies on ZrGeM (M = S, Se, and Te), from which we have revealed properties consistent with the theoretically predicted topological semimetal states. From the angular dependence of quantum oscillation frequency, we have also studied the Fermi surface topologies of these materials. Moreover, we have compared Dirac electron behavior between the ZrGeM and ZrSiM systems, which reveals deep insights to the tuning of Dirac state by spin-orbit coupling and lattice constants in the *WHM* system.

DOI: 10.1103/PhysRevB.95.205134

The discoveries of topological semimetals have opened a new era of condensed matter physics. These materials represent new topological states of quantum matter and exhibit exotic properties resulting from relativistic fermions hosted by Dirac or Weyl cones, such as extremely high bulk carrier mobility [1–7], large magnetoresistance [1–7], and potential topological superconductivity [8], which hold tremendous potential for technology applications. In three-dimensional (3D) Dirac semimetals such as Na_3Bi [9,10] and Cd_3As_2 [11–14], the fourfold degenerate band crossings at Dirac nodes are protected by the crystal symmetry. When the spin degeneracy is lifted by broken time reversal or spatial inversion symmetry, a Dirac state evolves to a Weyl state where each Dirac cone splits to a pair of Weyl cones with opposite chirality [9,11,15,16]. The inversion symmetry broken Weyl state has been demonstrated in transition metal monopnictides (Ta/Nb)(As/P) [15–22], photonic crystals [23], and $(W/Mo)Te_2$ [24–33]. The spontaneous time reversal symmetry breaking Weyl state has been reported in $YbMnBi_2$ [34] and magnetic Heusler alloys [35–41] and the magnetic members of R-Al-X (R = rare earth, X = Si, Ge) compounds [42].

In addition to the above topological semimetals with discrete Dirac/Weyl nodes in momentum space, another type of topological semimetal—the topological nodal line semimetal, which features Dirac bands crossing along a one-dimensional line/loop—has also been predicted [43–49] and experimentally observed in several material systems such as $(Pb/Tl)TaSe_2$ [50,51], ZrSiM (M = S, Se, Te) [52–56] and $PtSn_4$ [57]. Among these materials, the layered material ZrSiM exhibits unique properties. It hosts two types of Dirac states [52], i.e. the 3D nodal-line state with an exceptionally wide energy range of linear dispersion, and the two-dimensional (2D) Dirac state protected by the nonsymmorphic symmetry. The Dirac states were experimentally demonstrated by angle-resolved photoemission spectroscopy (ARPES) measurements [52,53] and quantum oscillation experiments for ZrSiS [58–61]. Replacing S by Se and Te greatly reduces the interlayer binding energy, but preserves the main topological signatures in the electronic structure [48]. Indeed, the topological Dirac nodal-line states in ZrSiSe and ZrSiTe have been experimentally demonstrated by quantum oscillation studies [54] and later confirmed by ARPES observations [55,56]. Furthermore, due to reduced interlayer binding, atomically thin 2D layers of ZrSiSe and ZrSiTe can be obtained by mechanical exfoliation (see supplement materials in Ref. [54]), which opens up the possibility to realize the predicted 2D topological insulator in monolayers [48] and provides a new platform for the investigation of new topological fermion physics in low dimensions.

ZrSiM compounds belong to a larger family of materials *WHM* with the PbFCl-type structure (W = Zr/Hf/La, H = Si/Ge/Sn/Sb, M = O/S/Se/Te) [48]. For the compounds with different combinations of W, H, and M elements, their overall electronic structures are predicted to be similar and display nodal-line states, besides some small discrepancies caused by the variations of spin-orbit coupling (SOC) strength and structural dimensionality [48]. Indeed, in addition to nodal-line states in the aforementioned ZrSiM [52–54,56], topologically nontrivial phases have also been observed in other *WHM*-type materials such as ZrSnTe [62] and HfSiS [63–65]. Given that the SOC strength and the structural dimensionality governed by the steric-electronic balance can be fine-tuned with different combinations of W, H, and M elements, *WHM* compounds provide an ideal platform to investigate the evolution of the topological fermion properties with these parameters. Therefore, experimental demonstrations and characterizations of the predicted topological states in other *WHM* compounds are important.

With the above motivation, we have extended our studies to the ZrGeM (M = S, Se, Te) system. Similar to other *WHM* compounds [48], ZrGeM also possesses a layered tetragonal structure formed from the stacking of M-Zr-Ge-Zr-M slabs [Fig. 1(a)] [66,67]. Compared to ZrSiM, ZrGeM has an enhanced interlayer binding energy [48]; hence, its electronic structure is expected to be more 3D. Although the first principle calculations have shown ZrGeM shares similar electronic structures near the Fermi level with ZrSiM [48], i.e. hosting topological Dirac nodal-line state, experimental verification

---

[*] jhu@tulane.edu
[†] zmao@tulane.edu

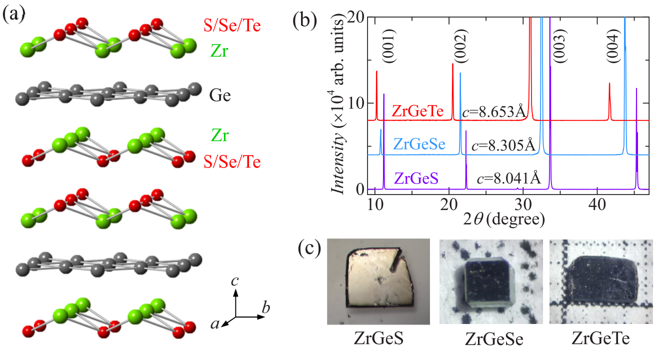

FIG. 1. (a) Crystal structure of ZrGeM (M = S, Se, Te). (b) Single crystal x-ray diffraction patterns for ZrGeM. (c) Images of ZrGeM single crystals.

has not been reported thus far. In this paper, we report quantum oscillation studies on ZrGeM compounds and show the features consistent with the predicted topological fermions in this family of materials.

The ZrGeM single crystals [Fig. 1(c)] were synthesized by a chemical vapor transport method similar to that used for growing ZrSiM single crystals [54,58]. The compositions of the synthesized crystals were analyzed using energy dispersive spectroscopy (EDS). The excellent crystallinity is demonstrated by the sharp (00L) x-ray diffraction peaks, as shown in Fig. 1(b). Due to the increased ionic radius from S to Te ions, the c-axis lattice parameter, i.e. the M-Zr-Ge-Zr-M slab thickness, is increased from 8.041 Å for ZrGeS to 8.305 Å for ZrGeSe and to 8.653 Å for ZrGeTe. A similar trend was also observed in the ZrSiM compounds [54].

Signatures of topological Dirac states in ZrGeM, including light effective mass, high mobility, and nontrivial Berry phase, have been found in our quantum oscillation experiments, which were performed using the 31T resistive magnet in NHMFL, Tallahassee. In our measurements, both Shubnikov–de Haas (SdH) and de Haas–van Alphen (dHvA) oscillations have been observed in ZrGeM. However, the SdH oscillations are much weaker than the dHvA oscillations (shown later). Our previous paper on ZrSiS has shown the dHvA effect better reveals intrinsic Dirac fermion properties [58]. Therefore, our analyses will be mainly focused on the dHvA effect, which was probed in magnetic torque measurements using a piezoresistive cantilever. Given the torque signal is expected to vanish when magnetic field is perfectly aligned along the out-of-plane ($B \parallel c$) and in-plane ($B \parallel ab$) directions, we performed the measurements with the fields nearly along the out-of-plane and in-plane directions (denoted by c' and ab', respectively). In Figs. 2(a) and 2(d), we have presented the field dependences of magnetic torque at different temperatures for ZrGeS for $B \parallel c'$ and $B \parallel ab'$, respectively. For both field orientations, we observed strong dHvA oscillations at low temperatures. The oscillations vanished when the temperature was increased above 30 K. The presence of quantum oscillations for both field orientations indicates a 3D Fermi surface in ZrGeS despite its layered crystal structure, which will be discussed in more detail later. From the oscillatory torque $\Delta\tau$ obtained by subtracting the smooth background [Figs. 2(b) and 2(e)], one can find that both oscillation patterns contain multiple frequency components. This can be clearly seen in the fast Fourier transform (FFT) analyses as shown in Figs. 2(c) and 2(f). The dHvA oscillations are composed of one lower frequency F_α (=12.5 T) and two higher frequencies $F_{\beta1}$(=236 T) and $F_{\beta2}$(=380 T) for $B \parallel c'$, and one low frequency F_α(=17 T) and one high frequency $F_{\beta1}$(=132 T) for $B \parallel ab'$. The coexistence of lower and higher frequencies has also been observed in ZrSiS [54,59,60] and HfSiS [64]. Given the relatively complex Fermi surfaces of WHM compounds [48], when magnetic field is applied along a symmetry axis, one observed oscillation frequency is possibly due to two Fermi surface pockets with nearly the same cross-section areas. If this is the case, these two Fermi surfaces can hardly be resolved by FFT. However, this scenario can be excluded by the measurements of the angular dependences of dHvA oscillations. Since the cross-section areas of different Fermi surfaces generally show different angular dependences, the splitting of the oscillation frequency with the rotation of magnetic field can be expected for the aforementioned scenario. As will be shown below, no such splitting has been observed for $F_\alpha, F_{\beta1}$, or $F_{\beta2}$.

For $B \parallel c'$, we have also observed splitting of oscillation peaks for the lower and higher frequency components at low temperature, as indicated by the black and purple arrows in Fig. 2(a), respectively. The split peaks gradually merge upon increasing temperature [Fig. 2(a)], which is a typical signature of Zeeman effect due to the broadening and overlapping of the split Landau levels at higher temperatures. Although our FFT analyses revealed multiple frequencies, from the careful inspection of the oscillation patterns [Fig. 2(a)], we can see that Zeeman splitting occurs for the $F_\alpha = 12.5$ T and $F_{\beta1} = 236$ T oscillation components. For the F_α component, due to the extremely low frequency and strong peak splitting, Zeeman effect could easily be overlooked and the split peaks could be mistakenly attributed to the normal oscillation peaks from unsplit Landau levels. Fortunately, clear signatures of Zeeman effect can be resolved in susceptibility oscillations (dM/dB), which are obtained by taking the derivative of the lower frequency component due to $\tau \propto M$, as shown in the inset of Fig. 2(b). Similar features are also observed in ZrSiS, in which the dHvA oscillations have clearly revealed Zeeman splitting [58], which was not resolved in the SdH oscillations [59,60]. From the peak splitting and the effective electron mass (see below), we have evaluated the g factor of quasiparticles using a method discussed in Ref. [58]; $g = 15$ and 12, respectively, for the quasiparticles hosted by the F_α and $F_{\beta1}$ bands, much larger than the g factor of a free electron ($g \sim 2$). This result is consistent with our previous observation of strong Zeeman splitting with a large g factor (∼38) in ZrSiS [58].

More information about the Dirac fermions properties in ZrGeS can be extracted from the analyses of dHvA oscillations. The dHvA oscillations for a 3D system can be described by the 3D Lifshitz-Kosevich (LK) formula [68,69] with a Berry phase being taken into account for a topological system [70]:

$$\Delta\tau \propto -B^{1/2} R_T R_D R_S \sin\left[2\pi\left(\frac{F}{B} + \gamma - \delta\right)\right], \quad (1)$$

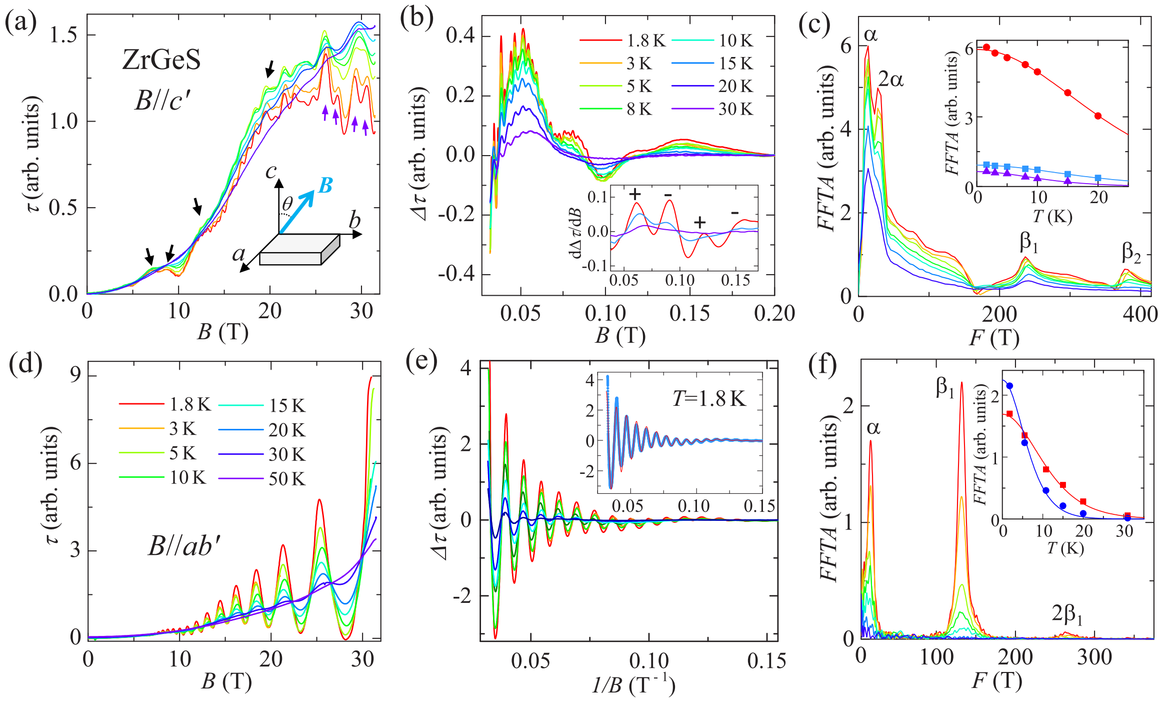

FIG. 2. (a) The field dependence of magnetic torque τ for ZrGeS at different temperatures, which displays strong dHvA oscillations. The magnetic field is applied along the nearly out-of-plane direction ($B \parallel c'$). The black and purple arrows indicate the splitting of oscillation peaks for the F_α(=12.5 T) and $F_{\beta 1}$(=236 T) components. Inset: the experiment setup. (b) The oscillatory component of τ for $B \parallel c'$. Inset: Zeeman splitting in susceptibility oscillations at $T = 1.8$, 15, and 30 K. (c) The FFT spectra for the oscillatory component $\Delta\tau$ for $B \parallel c'$. Inset: the temperature dependence of the FFT amplitude of the major fundamental frequencies and the fits to the LK formula (solid lines). (d) The field dependence of magnetic torque τ for ZrGeS at different temperatures. The magnetic field is applied along the nearly in-plane direction ($B \parallel ab'$). (e) The oscillatory component of τ for $B \parallel ab'$. Inset: the fit of the oscillation pattern at $T = 1.8$ K to the multiband LK formula. (f) The FFT spectra for the oscillatory component $\Delta\tau$ for $B \parallel c'$. Inset: the temperature dependence of the FFT amplitude of the major fundamental frequencies and the fit to the LK formula (solid lines).

where $R_T = \alpha T\mu/B\sinh(\alpha T\mu/B)$, $R_D = \exp(-\alpha T_D\mu/B)$, and $R_S = \cos(\pi g\mu/2)$. Here, $\mu = m^*/m_0$ is the ratio of effective cyclotron mass m^* to free electron mass m_0. Also, T_D is Dingle temperature, and $\alpha = (2\pi^2 k_B m_0)/(\hbar e)$. The oscillations of $\Delta\tau$ are described by the sine term with a phase factor $\gamma - \delta$, in which $\gamma = \frac{1}{2} - \frac{\phi_B}{2\pi}$ and ϕ_B is Berry phase. The phase shift δ is determined by the dimensionality of the Fermi surface and has a value of $\pm 1/8$ for 3D cases, with the sign depending on whether the probed extreme cross-section area of the FS is maximal (−) or minimal (+) [68]. From the LK formula, the effective mass m^* can be obtained through the fit of the temperature dependence of the oscillation amplitude to the thermal damping factor R_T. In the case of multifrequency oscillations, the oscillation amplitude for each frequency can be represented by the amplitude of FFT peak, and the parameter $1/B$ in R_T should be the average inverse field $1/\bar{B}$, defined as $1/\bar{B} = (1/B_{max} + 1/B_{min})/2$, where B_{max} and B_{min} define the magnetic field range used for FFT. As shown in the insets of Figs. 1(c) and 1(f), for all probed oscillation frequencies, the obtained effective masses are in the range of 0.05–0.1 m_0 (see Table I), which are only slightly larger than those obtained from the dHvA oscillation studies on ZrSiS [58], and agrees with the nature of massless relativistic fermions.

High quantum mobility and π Berry phase are also important characteristics of topological fermions. For the multifrequency oscillations seen in ZrGeS, these parameters cannot be directly obtained through the conventional approaches, i.e. the Dingle plot and the Landau level fan diagram, but can be extracted through the fit of the oscillation pattern to the

TABLE I. Parameters derived from the analyses of dHvA oscillations for ZrGeS. F, oscillation frequency; T_D, Dingle temperature; m^*, effective mass; τ, quantum relaxation time; μ_q, quantum mobility; ϕ_B, Berry phase.

	F (T)	m^*/m_0	T_D (K)	τ (ps)	μ (cm^2/Vs)	ϕ_B
$B\parallel c'$	12.5	0.05				
	236	0.062				
	380	0.097				
$B\parallel ab'$	17	0.05	28	0.044	1547	$[-0.38(3) \pm 0.25]\pi$
	132	0.09	35	0.035	684	$[-0.22(5) \pm 0.25]\pi$

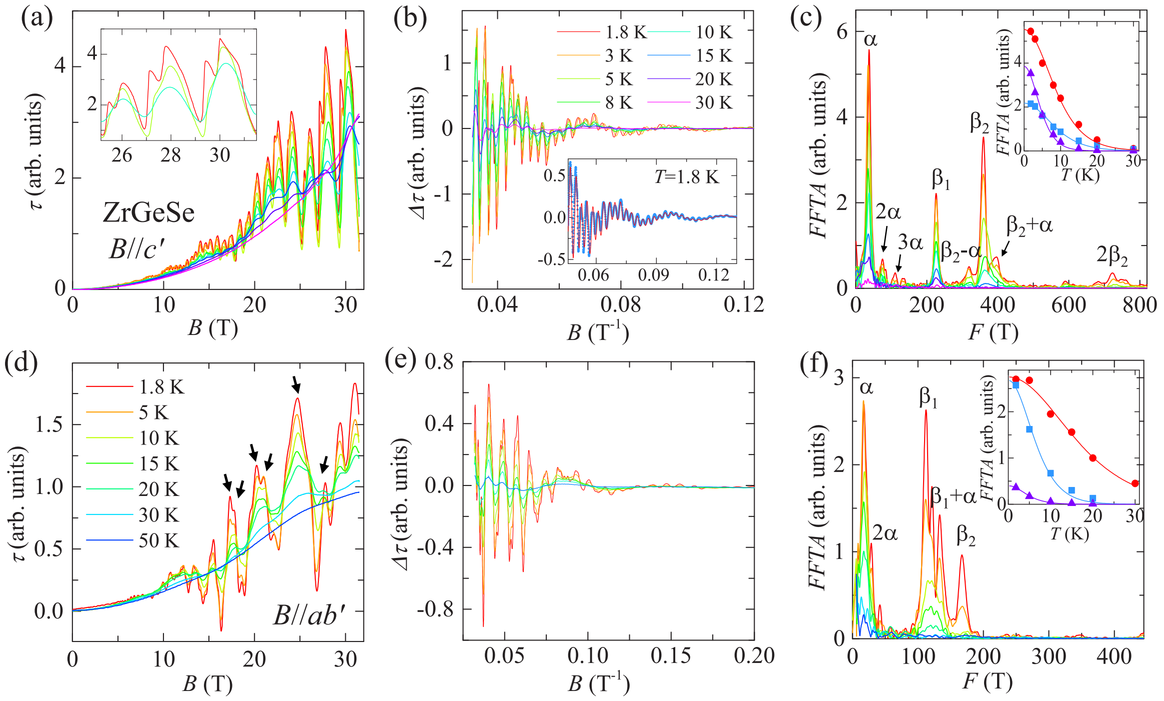

FIG. 3. (a) The field dependence of magnetic torque τ for ZrGeSe at different temperatures for $B \parallel c'$. Inset: dHvA oscillations in τ under high field, which displays inverse sawtooth pattern and Zeeman splitting. (b) The oscillatory component of τ for $B \parallel c'$. Inset: the fit of the oscillation pattern at $T = 1.8$ K to the multiband LK formula. (c) The FFT spectra for the oscillatory component $\Delta\tau$ for $B \parallel c'$. Inset: the temperature dependence of the FFT amplitude of the major fundamental frequencies and the fits to the LK formula (solid lines). (d) The field dependence of magnetic torque τ for ZrGeSe at different temperatures for $B \parallel ab'$. The black arrows indicate split peaks. (e) The oscillatory component of τ for $B \parallel ab'$. (f) The FFT spectra for the oscillatory component $\Delta\tau$ for $B \parallel c'$. Inset: the temperature dependence of the FFT amplitude of the major fundamental frequencies and the fits to the LK formula (solid lines).

generalized multiband LK formula [71]. This method has been shown to be efficient for the analyses of the multifrequency quantum oscillations in ZrSiM [54,58]. The LK fit to the $T = 1.8$ K oscillation pattern is very difficult for the case of $B \parallel c'$ due to the presence of a strong Zeeman effect, but much easier for $B \parallel ab'$, as shown in the inset of Fig. 2(e). As summarized in Table I, from the LK fit for $B \parallel ab'$, we have obtained Dingle temperatures of 28 and 35 K, respectively, for the lower (17 T) and higher frequencies (132 T). The quantum relaxation time $\tau_q[=\hbar/(2\pi k_B T_D)]$ corresponding to such values of Dingle temperature are 4.4×10^{-14} s and 3.5×10^{-14} s, from which the quantum mobility $\mu_q(=e\tau/m^*)$ are estimated to be 1547 and 684 cm^2/Vs, respectively. The obtained quantum mobility values for ZrGeS are remarkably smaller than those of ZrSiS (2000–10000 cm^2/Vs [58]). Given that high mobility is the generic feature of topological relativistic fermions [1], the low quantum mobility seen in ZrGeS may imply that replacing Si by Ge results in some changes in Dirac crossings in band structure, which will be discussed in more details below.

The relativistic nature of carriers is supported by the nontrivial Berry phases. The Landau index fan diagram has been commonly used for Berry phase determination. Precise determination of Berry phase using this method requires that the system has a single frequency and lower index Landau levels can be reached. When the measured field range is far from reaching the quantum limit, the Berry phase obtained using the fan diagram could have a large uncertainty [72,73]. This is because, in this method, Berry phase is determined by the intercept of the linear extrapolation of the Landau level index plot (i.e., $\phi_B = 2\pi \times$ intercept). Such an extracted intercept is greatly affected by the slope of the extrapolated linear line. A very small variation of the slope can lead to a big change in the intercept [72]. However, in the LK fit of the oscillation pattern, a small variation of phase factor can lead to observable mismatch between the fitted curve and the data points. Therefore, LK fit provides an alternative approach for the determination of Berry phase, which is particularly useful for the multifrequency oscillations. From the LK fit, we obtained the phase factors $(\gamma - \delta)$ of 0.69 and 0.61 for the F_α and $F_{\beta 1}$ bands, respectively, from which the Berry phases are found be $[-0.38(3) \pm 0.25]$ and $[-0.22(5) \pm 0.25]\pi$, respectively (Table I). Such results are consistent with the theoretically predicted topological Dirac states in all *WHM* systems [48].

Similar features of topological fermions have also been seen in the isostructural compounds ZrGeSe and ZrGeTe. We also observed strong dHvA oscillations in magnetic torque measurements on ZrGeSe [Figs. 3(a) and 3(d)] and ZrGeTe [Figs. 4(a) and 4(d)]. Like ZrGeS, ZrGeSe also exhibits dHvA oscillations with multiple frequencies for both $B \parallel c'$ [Fig. 3(b)] and $B \parallel ab'$ [Fig. 3(e)], which are clearly resolved in FFT spectra [Figs. 3(c) and 3(f)]. In the FFT spectra, a magnetic breakdown effect is observed. This effect is caused by quantum tunneling of electrons between the different orbits on the different parts of Fermi surface [69], leading

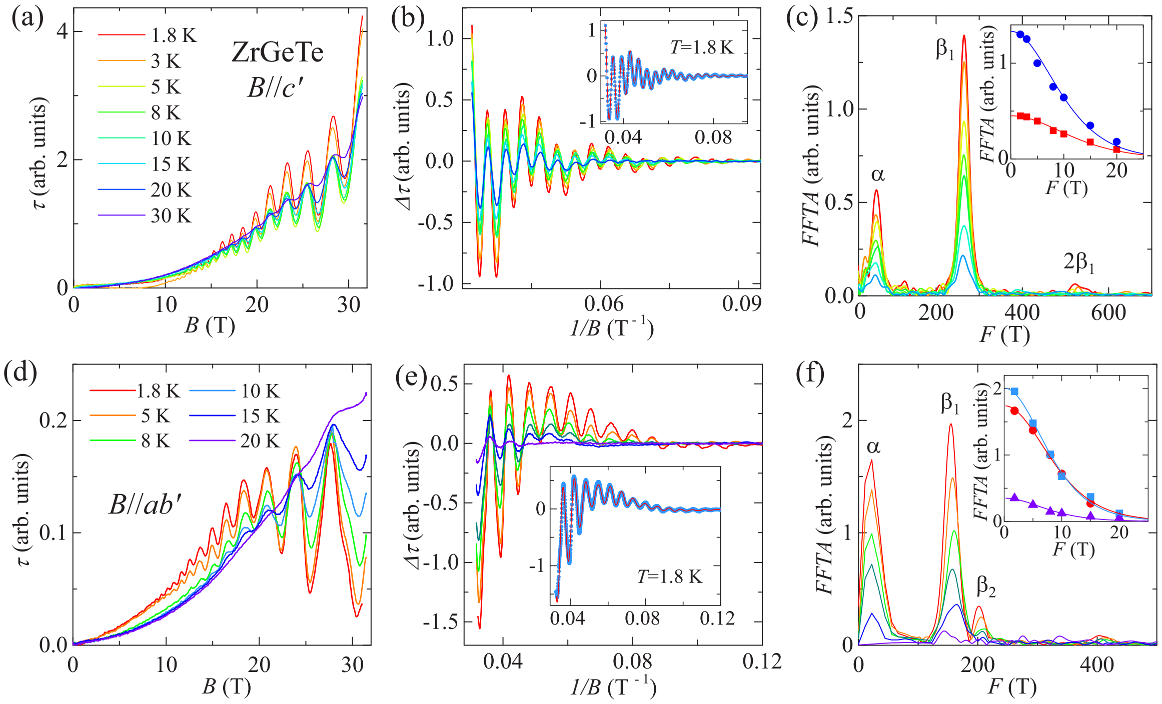

FIG. 4. (a) The field dependence of magnetic torque τ for ZrGeTe at different temperatures for $B \parallel c'$. (b) The oscillatory component of τ for $B \parallel c'$. Inset: the fit of the oscillation pattern at $T = 1.8$ K to the multiband LK formula. (c) The FFT spectra for the oscillatory component $\Delta\tau$ for $B \parallel c'$. Inset: the temperature dependence of the FFT amplitude of the major fundamental frequencies and the fits to the LK formula (solid lines). (d) The field dependence of magnetic torque τ for ZrGeTe at different temperatures for $B \parallel ab'$. (e) The oscillatory component of τ for $B \parallel ab'$. Inset: the fit of the oscillation pattern at $T = 1.8$ K to the multiband LK formula. (f) The FFT spectra for the oscillatory component $\Delta\tau$ for $B \parallel c'$. Inset: the temperature dependence of the FFT amplitude of the major fundamental frequencies and the fits to the LK formula (solid lines).

to additional frequencies equal to the sum or difference of fundamental frequencies, as shown in Figs. 3(c) and 3(f). In addition to the magnetic breakdown, Zeeman splitting also appears at high field for both $B \parallel c'$ and $B \parallel ab'$, manifesting itself in peak splitting, as shown in the inset of Fig. 3(a) and indicated by the arrows in Fig. 3(d). In contrast with ZrGeS, which displays strong splitting for both lower and higher frequency components when $B \parallel c'$ [Fig. 2(a)], Zeeman splitting in ZrGeSe can be observed for both $B \parallel c'$ and $B \parallel ab'$ and is resolvable only for the higher frequency component. Due to too many oscillation frequencies in ZrGeSe, we are unable to tell which frequency components exhibit Zeeman splitting, hence the values of g factor cannot be determined. Another interesting feature in ZrGeSe is the inverse sawtooth-like oscillation pattern at low temperatures for $B \parallel c'$ [Fig. 3(a), inset], which is suggestive of a 2D/quasi-2D electronic state in some cases [69,74]. Nevertheless, we note that inverse sawtoothlike oscillation pattern could also be caused by the torque interaction, which is essentially an instrumental effect due to the feedback of the oscillating magnetic moment on the cantilever position [75]. Our observed inverse sawtoothlike oscillations most likely have this origin, since we did not observe such inverse sawtoothlike oscillations in ZrGeTe, whose electronic structure should have lower dimensionality than ZrGeSe, as discussed below.

For the major fundamental frequencies seen in FFT spectra [Figs. 3(c) and 3(f)], from the fit of the temperature dependence of FFT amplitude [insets of Figs. 3(c) and 3(f)], the effective masses are estimated to be ∼0.05–0.22 m_0 (Table II), larger than those for ZrGeS (Table I). Through the multiband LK fit, we can also obtain the quantum mobility and Berry phase of quasiparticles in ZrGeSe. For $B \parallel c'$, the fit was limited to the magnetic field range below $B = 20$ T [Fig. 3(b), inset] to avoid the complexity induced by strong Zeeman splitting at high fields. For $B \parallel ab'$, however, the fitting was not successful due to the complicated oscillation pattern. From the multiband LK fit to the oscillation pattern of $B \parallel c'$ at 1.8 K [Fig. 3(b), inset], we have obtained quantum mobility ranging from 392–1630 cm^2/Vs, lower than that in ZrGeS (Table I). In spite of that, we have obtained nontrivial Berry phases for the $F = 37.4$ T and 360 T bands, implying that the topological nontrivial states also exist in ZrGeSe. Table II summarizes all the fitted parameters, including the quantum mobility and Berry phases.

For the case of ZrGeTe, its dHvA oscillations display relatively simpler patterns as compared to ZrGeS and ZrGeSe, without signatures of Zeeman splitting or magnetic breakdown for both $B \parallel c'$ [Figs. 4(a)–4(c)] and $B \parallel ab'$ [Figs. 4(d)–4(f)]. The effective mass for each frequency component obtained from the fit of the temperature dependence of FFT amplitude [insets of Figs. 4(c) and 4(f)] ranges from 0.16 m_0 to 0.24 m_0, larger than those for ZrGeS and ZrGeSe. The oscillation patterns for both $B \parallel c'$ and $B \parallel ab'$ can be easily fitted to the multiband LK formula, as shown in the insets of Figs. 4(b)

TABLE II. Parameters derived from the analyses of dHvA oscillations for ZrGeSe. F, oscillation frequency; T_D, Dingle temperature; m^*, effective mass; τ, quantum relaxation time; μ_q, quantum mobility; ϕ_B, Berry phase.

	F (T)	m^*/m_0	T_D (K)	τ (ps)	μ (cm^2/Vs)	ϕ_B
$B\|c'$	37.4	0.11	12	0.102	1630	$[0.78(3) \pm 0.25]\pi$
	226	0.22	25	0.049	392	$[-0.28(6) \pm 0.25]\pi$
	360	0.12	35	0.035	513	$[1.21(3) \pm 0.25]\pi$
$B\|ab'$	17.3	0.05				
	112	0.13				
	167	0.17				

and 4(e), from which we have obtained nontrivial Berry phases for each band (Table III).

From the above analyses, we have revealed evidence of topological fermions in ZrGeM (M = S, Se, Te), including light effective mass, high quantum mobility, and nontrivial Berry phases. These results are consistent with the theoretically predicted topological nodal-line state in *WHM* compounds [48]. From ZrGeS to ZrGeTe, the interlayer binding energy is predicted to become smaller [48] so that we can expect a possible evolution toward 2D in the electronic structure. In order to better understand the dimensionality evolution of the electronic structure in the ZrGeM series, we have studied the angular dependence of the quantum oscillations, which can reveal direct information on the Fermi surface morphology.

Using the measurement setup shown in the inset of Fig. 2(a), we have measured dHvA oscillations for the ZrGeM compounds under different field orientations. After the background subtraction, the oscillation pattern of $\Delta\tau$ displays a clear evolution with the rotation of the magnetic field for each member in ZrGeM, as shown in Figs. 5(a)–5(c). In Figs. 5(d)–5(f), we present the angular dependences of the major fundamental frequencies obtained from the FFT analyses. As a cross check, we have also studied the SdH effect in ZrGeM through magnetotransport measurements. As shown in Fig. 6, SdH oscillations can be observed for the out-of-plane field orientations ($B \parallel c$). For in-plane fields ($B \parallel ab$), the SdH effect is hardly visible for all three compounds. Furthermore, we have observed negative longitudinal magnetoresistance for ZrGeS, which is a sign of chiral anomaly that has been observed in other Dirac materials [1,76], or possibly associated with the inhomogeneous current flow in high mobility materials with field-induced resistance anisotropy (i.e., the current-jetting effect) [77,78]. The attenuation of the SdH effect with the field rotating toward the in-plane direction has also been observed in ZrSiM [52,54], which seems to be a generic feature for all the *WHM*-type nodal-line semimetals. In spite of that, in the angular range where SdH oscillations are observable, the extracted SdH oscillation frequencies and their angular dependences agree well with those measured in the dHvA oscillations [Figs. 5(d)–5(f)], though some high frequency components are too weak to be probed.

As shown in Figs. 5(d)–5(f), in all the three ZrGeM compounds, we find the high frequency branch is composed of $F_{\beta1}$ and $F_{\beta2}$. The difference between $F_{\beta2}$ and $F_{\beta2}$ varies remarkably with angle, reaching zero at certain angles, which is suggestive of corrugated cylindrical Fermi surfaces, as widely seen in other quasi-2D systems such as iron-based superconductors [79], and agrees with the layered structure of ZrGeM [Fig. 1(a)]. However, the presence of dHvA oscillations in the whole angle range from $\theta = 0$ to 90° clearly indicates 3D Fermi surface. Therefore, the Fermi surface composed of $F_{\beta1}/F_{\beta2}$ bands should be highly anisotropic. In contrast, the Fermi surface comprised of the F_α band is less anisotropic, which is reflected in the weak angular dependence of F_α [Figs. 5(d)–5(f)]. The 3D characters of both $F_{\beta1}/F_{\beta2}$ and F_α bands can be attributed to strong interlayer binding energy in ZrGeM [48]. For instance, the binding energy in ZrGeTe is nearly three times higher than that of ZrSiTe [48]. For these three major frequencies $F_\alpha, F_{\beta1}$, and $F_{\beta2}$, we did not observe clear splitting in their angular dependences, implying that each of these frequencies is not due to different Fermi surfaces with nearly the same cross-section areas as mentioned above. To further map out the precise morphology of the 3D Fermi surface, theoretical and ARPES studies are needed.

Given that ZrSiM and ZrGeM are expected to share similar electronic band structures near the Fermi level [48], the comparison between these two families of compounds can provide further information on the nature of the electronic bands probed in the quantum oscillations in ZrGeM. As noted above, in the ZrSiM family, ZrSiS has been found to harbor a 3D nodal-line state with a very small SOC-induced gap (∼20 meV), as well as a gapless 2D Dirac cone state protected by the nonsymmorphic symmetry [52]. The

TABLE III. Parameters derived from the analyses of dHvA oscillations for ZrGeTe. F, oscillation frequency; T_D, Dingle temperature; m^*, effective mass; τ, quantum relaxation time; μ_q, quantum mobility; ϕ_B, Berry phase.

	F (T)	m^*/m_0	T_D (K)	τ (ps)	μ (cm^2/Vs)	ϕ_B
$B\|c'$	62	0.16	30	0.041	451	$[1.20(4) \pm 0.25]\pi$
	265	0.20	27	0.046	404	$[0.44(6) \pm 0.25]\pi$
$B\|ab'$	13	0.21	14.4	0.086	720	$[-1.08(6) \pm 0.25]\pi$
	156	0.23	14.6	0.084	640	$[0.60(4) \pm 0.25]\pi$
	203	0.24	16	0.077	564	$[0.70(7) \pm 0.25]\pi$

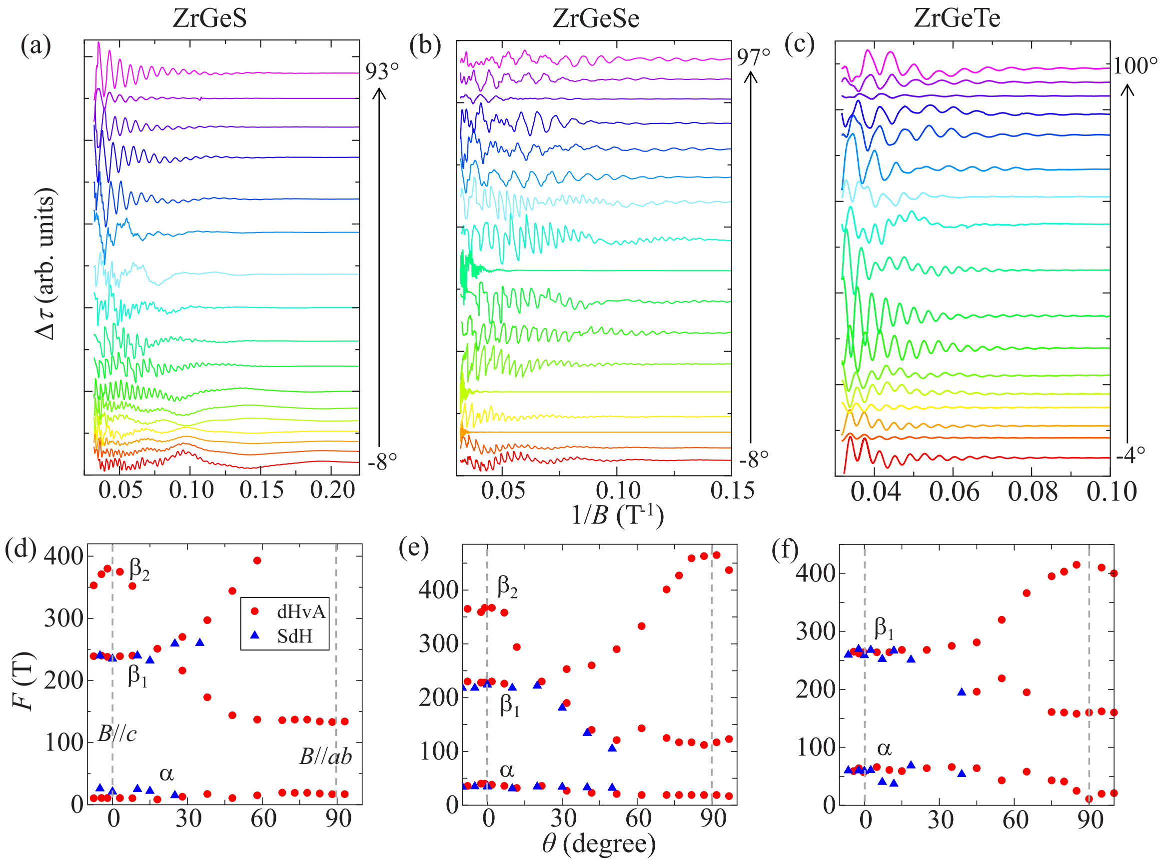

FIG. 5. dHvA oscillations of (a) ZrGeS, (b) ZrGeSe, and (c) ZrGeTe at $T = 1.8$ K under different magnetic field orientations. The data collected under at different θ have been shifted for clarity. The angular dependence of oscillation frequencies for (d) ZrGeS, (e) ZrGeSe, and (f) ZrGeTe. The gray dashed lines indicate the in-plane ($B \parallel c$, 0°) and out-of-plane ($B \parallel ab$, 90°) directions.

nodal-line bands is expected to give rise to both the high (F_β) and low (F_α) frequency dHvA oscillations, respectively [58]. For the ZrGe*M* compounds, as presented above, our dHvA experiments also reveal high and low frequency oscillation components with nontrivial Berry phase (Tables I–III). The higher frequencies are in the 112–380 T range (see Tables I–III), which is of the same order of magnitude as that in ZrSi*M* (102–240 T) [54,58]. This fact, together with their angular dependences [Figs. 5(d)–5(f)], suggests that those higher frequency oscillation components most likely originate from the 3D nodal-line Dirac bands. For the lower frequency component (F_α), considering the strong 3D character, one possible origin for such a low frequency band is the Fermi surface comprised of topological trivial bands, which is predicted in the first principle calculations and found to display 3D character [48,55]. However, the observed light effective mass, high quantum mobility, and nontrivial Berry phase are inconsistent with such a topologically trivial band. Similarly, a low frequency oscillation component with 3D character is also probed in the quantum oscillation studies for a *WHM* compound HfSiS [64]. Such low frequency component has been ascribed to the topological nontrivial bands though the trivial band is also found in the first principle calculations [48,55]. Therefore, to further clarify the nature of the F_α band in ZrGe*M*, more theoretical and experimental efforts are necessarily needed.

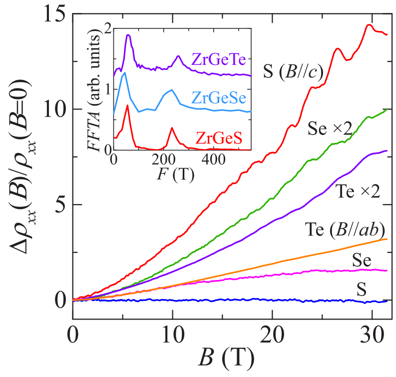

FIG. 6. In-plane magnetoresistance and SdH oscillations of ZrGe*M* (*M* = S, Se, Te) for $B \parallel c$ and $B \parallel ab$. The data for ZrGeSe and ZrGeTe for $B \parallel c$ have been multiplied by a factor of 2 for clarity. Inset: The FFT spectra for the SdH oscillations; the data have been shifted for clarity.

In addition to the dimensionality difference between ZrGe*M* and ZrSi*M*, the greater ionic radius of Ge is also expected to modify lattice constants, thus affecting the electronic structure [80]. Moreover, the SOC strength is also stronger in ZrGe*M* due to the fact that the Ge atom is heavier than the Si atom. Therefore, ZrGe*M* provides a good platform for examining how these parameters affect the topological fermion properties in the *WHM*-type materials. Previous studies have shown that the lattice constant ratio c/a in *WHM* governs the

Dirac node position for the nonsymmorphic Dirac cone [55]. The c/a ratio can be tuned by M since the c axis elongates for larger M atoms [Fig. 1(a)]. In ZrSiS, which shows a small $c/a \sim 2.27$ [80], the nonsymmorphic bands cross below the Fermi level [52], whereas in ZrSiTe, due to the right c/a ratio (∼2.57), the nonsymmorphic Dirac bands cross right at the Fermi level, which allows for investigating the transport properties of the Dirac fermions protected by the nonsymmorphic symmetry [55]. Nevertheless, under such a circumstance, the zeroth Landau level of the relativistic fermions is pinned at the Dirac node, and other Landau levels would not pass through the Fermi level upon increasing magnetic field [81], so the quantum oscillations due to the nonsymmorphic Dirac fermions were not detected in our previous dHvA experiments on ZrSiTe [54]. In addition to the tuning through the M atom, the c/a ratio is also affected by H since the a axis is determined by the square net formed by H atoms [Fig. 1(a)]. Due to the larger ionic radius of Ge, substituting Ge for Si is equivalent to applying lateral tensile strain, thus resulting in even smaller c/a ratios (∼2.21, 2.23, and 2.22 for M = S, Se, and Te, respectively) in ZrGeM than in ZrSiS, so the Dirac node of the nonsymmorphic Dirac cone in ZrGeM may be pushed further away from the Fermi level. As a result, the Fermi pocket formed by such Dirac bands is expected to be larger, which is consistent with our experimental observation that F_α probed in ZrGeM (12–62 T for $B \parallel c'$) is larger than that the F_α value in ZrSiS (8.4T for $B \parallel c$) [58].

In ZrSiS, the nonsymmorphic Dirac cone generated by the Si square lattice does not show a SOC-induced gap due to the protection by the nonsymmorphic symmetry, while the nodal-line is gapped by SOC [48,52]. Given that the effective mass of Dirac fermions is determined by the Fermi velocity v_F (i.e., $m^* = \varepsilon_F/v_F^2$), the opening of the SOC-induced gap leads the energy band to deviate from linear dispersion, thus resulting in a decrease in the Fermi velocity and consequently the increase of effective mass. In ZrSiM, from M = S to Se and to Te, the nodal-line Dirac fermions become more massive and quantum mobility becomes lower [54,58], which is in line with enhanced SOC-induced gaps due to heavier elements [55]. A similar trend is also observed for the high frequency band (which corresponds to the nodal-line band, as discussed above) in ZrGeM (Tables I–III). Furthermore, as noted above, SOC in ZrGeM should be stronger than in ZrSiM for the identical M atom. Indeed, our experimental results presented above show that, for each M atom (S, Se, or Te), the effective cyclotron mass is heavier and the quantum mobility is lower in ZrGeM (Tables I–III) than in ZrSiM [54,58]. Another possible interpretation for the lower quantum mobility in ZrGeM materials is the different impurity concentrations for the Si- and Ge-based compounds.

In summary, we have synthesized the single crystals of ZrGeM (M = S, Se, and Te) and performed quantum oscillation studies on these materials. The analyses of dHvA quantum oscillation data reveal properties consistent with the theoretically predicted topological semimetal state in ZrGeM for the first time. The Fermi surfaces comprised of Dirac bands exhibit the 3D nature for all the ZrGeM compounds, due to enhanced interlayer binding energy. From the comparison between the ZrGeM and ZrSiM systems, we find that the topological fermion properties can be tuned by lattice constant and SOC through different combination of elements. These findings provide clues to the design and tuning of topological Dirac state in the *WHM*-based materials.

This work was supported by the US Department of Energy under Grant No. DE-SC0014208 (support for personnel, material synthesis, and magnetization measurements). The work at the National High Magnetic Field Laboratory is supported by the NSF Cooperative Agreement No. DMR-1157490 and the State of Florida (high field magnetic torque and magnetotransport measurements).

---

[1] T. Liang, Q. Gibson, M. N. Ali, M. Liu, R. J. Cava, and N. P. Ong, Nat. Mater. **14**, 280 (2015).

[2] J. Xiong, S. Kushwaha, J. Krizan, T. Liang, R. J. Cava, and N. P. Ong, Europhys. Lett. **114**, 27002 (2016).

[3] C. Shekhar, A. K. Nayak, Y. Sun, M. Schmidt, M. Nicklas, I. Leermakers, U. Zeitler, Y. Skourski, J. Wosnitza, Z. Liu, Y. Chen, W. Schnelle, H. Borrmann, Y. Grin, C. Felser, and B. Yan, Nat. Phys. **11**, 645 (2015).

[4] N. J. Ghimire, L. Yongkang, M. Neupane, D. J. Williams, E. D. Bauer, and F. Ronning, J. Phys. Condens. Matter **27**, 152201 (2015).

[5] Z. Wang, Y. Zheng, Z. Shen, Y. Lu, H. Fang, F. Sheng, Y. Zhou, X. Yang, Y. Li, C. Feng, and Z.-A. Xu, Phys. Rev. B **93**, 121112 (2016).

[6] F. Arnold, C. Shekhar, S.-C. Wu, Y. Sun, R. D. dos Reis, N. Kumar, M. Naumann, M. O. Ajeesh, M. Schmidt, A. G. Grushin, J. H. Bardarson, M. Baenitz, D. Sokolov, H. Borrmann, M. Nicklas, C. Felser, E. Hassinger, and B. Yan, Nat. Commun. **7**, 11615 (2016).

[7] X. Huang, L. Zhao, Y. Long, P. Wang, D. Chen, Z. Yang, H. Liang, M. Xue, H. Weng, Z. Fang, X. Dai, and G. Chen, Phys. Rev. X **5**, 031023 (2015).

[8] H. Wang, H. Wang, H. Liu, H. Lu, W. Yang, S. Jia, X.-J. Liu, X. C. Xie, J. Wei, and J. Wang, Nat. Mater. **15**, 38 (2016).

[9] Z. Wang, Y. Sun, X.-Q. Chen, C. Franchini, G. Xu, H. Weng, X. Dai, and Z. Fang, Phys. Rev. B **85**, 195320 (2012).

[10] Z. K. Liu, B. Zhou, Y. Zhang, Z. J. Wang, H. M. Weng, D. Prabhakaran, S.-K. Mo, Z. X. Shen, Z. Fang, X. Dai, Z. Hussain, and Y. L. Chen, Science **343**, 864 (2014).

[11] Z. Wang, H. Weng, Q. Wu, X. Dai, and Z. Fang, Phys. Rev. B **88**, 125427 (2013).

[12] S. Borisenko, Q. Gibson, D. Evtushinsky, V. Zabolotnyy, B. Büchner, and R. J. Cava, Phys. Rev. Lett. **113**, 027603 (2014).

[13] Z. K. Liu, J. Jiang, B. Zhou, Z. J. Wang, Y. Zhang, H. M. Weng, D. Prabhakaran, S. K. Mo, H. Peng, P. Dudin, T. Kim, M. Hoesch, Z. Fang, X. Dai, Z. X. Shen, D. L. Feng, Z. Hussain, and Y. L. Chen, Nat. Mater. **13**, 677 (2014).

[14] M. Neupane, S.-Y. Xu, R. Sankar, N. Alidoust, G. Bian, C. Liu, I. Belopolski, T.-R. Chang, H.-T. Jeng, H. Lin, A. Bansil, F. Chou, and M. Z. Hasan, Nat. Commun. **5**, 3786 (2014).

[15] H. Weng, C. Fang, Z. Fang, B. A. Bernevig, and X. Dai, Phys. Rev. X **5**, 011029 (2015).

[16] S.-M. Huang, S.-Y. Xu, I. Belopolski, C.-C. Lee, G. Chang, B. Wang, N. Alidoust, G. Bian, M. Neupane, C. Zhang, S. Jia, A. Bansil, H. Lin, and M. Z. Hasan, Nat. Commun. **6**, 7373 (2015).

[17] S.-Y. Xu, I. Belopolski, N. Alidoust, M. Neupane, G. Bian, C. Zhang, R. Sankar, G. Chang, Z. Yuan, C.-C. Lee, S.-M. Huang, H. Zheng, J. Ma, D. S. Sanchez, B. Wang, A. Bansil, F. Chou, P. P. Shibayev, H. Lin, S. Jia *et al.*, Science **349**, 613 (2015).

[18] B. Q. Lv, H. M. Weng, B. B. Fu, X. P. Wang, H. Miao, J. Ma, P. Richard, X. C. Huang, L. X. Zhao, G. F. Chen, Z. Fang, X. Dai, T. Qian, and H. Ding, Phys. Rev. X **5**, 031013 (2015).

[19] B. Q. Lv, N. Xu, H. M. Weng, J. Z. Ma, P. Richard, X. C. Huang, L. X. Zhao, G. F. Chen, C. E. Matt, F. Bisti, V. N. Strocov, J. Mesot, Z. Fang, X. Dai, T. Qian, M. Shi, and H. Ding, Nat. Phys. **11**, 724 (2015).

[20] L. X. Yang, Z. K. Liu, Y. Sun, H. Peng, H. F. Yang, T. Zhang, B. Zhou, Y. Zhang, Y. F. Guo, M. Rahn, D. Prabhakaran, Z. Hussain, S. K. Mo, C. Felser, B. Yan, and Y. L. Chen, Nat. Phys. **11**, 728 (2015).

[21] S.-Y. Xu, N. Alidoust, I. Belopolski, Z. Yuan, G. Bian, T.-R. Chang, H. Zheng, V. N. Strocov, D. S. Sanchez, G. Chang, C. Zhang, D. Mou, Y. Wu, L. Huang, C.-C. Lee, S.-M. Huang, B. Wang, A. Bansil, H.-T. Jeng, T. Neupert *et al.*, Nat. Phys. **11**, 748 (2015).

[22] N. Xu, H. M. Weng, B. Q. Lv, C. E. Matt, J. Park, F. Bisti, V. N. Strocov, D. Gawryluk, E. Pomjakushina, K. Conder, N. C. Plumb, M. Radovic, G. Autes, O. V. Yazyev, Z. Fang, X. Dai, T. Qian, J. Mesot, H. Ding, and M. Shi, Nat. Commun. **7**, 11006 (2015).

[23] L. Lu, Z. Wang, D. Ye, L. Ran, L. Fu, J. D. Joannopoulos, and M. Soljačić, Science **349**, 622 (2015).

[24] A. A. Soluyanov, D. Gresch, Z. Wang, Q. Wu, M. Troyer, X. Dai, and B. A. Bernevig, Nature **527**, 495 (2015).

[25] Y. Sun, S.-C. Wu, M. N. Ali, C. Felser, and B. Yan, Phys. Rev. B **92**, 161107 (2015).

[26] F. Y. Bruno, A. Tamai, Q. S. Wu, I. Cucchi, C. Barreteau, A. de la Torre, S. McKeown Walker, S. Riccò, Z. Wang, T. K. Kim, M. Hoesch, M. Shi, N. C. Plumb, E. Giannini, A. A. Soluyanov, and F. Baumberger, Phys. Rev. B **94**, 121112 (2016).

[27] C. Wang, Y. Zhang, J. Huang, S. Nie, G. Liu, A. Liang, Y. Zhang, B. Shen, J. Liu, C. Hu, Y. Ding, D. Liu, Y. Hu, S. He, L. Zhao, L. Yu, J. Hu, J. Wei, Z. Mao, Y. Shi *et al.*, Phys. Rev. B **94**, 241119 (2016).

[28] Y. Wu, D. Mou, N. H. Jo, K. Sun, L. Huang, S. L. Bud'ko, P. C. Canfield, and A. Kaminski, Phys. Rev. B **94**, 121113(R) (2016).

[29] K. Deng, G. Wan, P. Deng, K. Zhang, S. Ding, E. Wang, M. Yan, H. Huang, H. Zhang, Z. Xu, J. Denlinger, A. Fedorov, H. Yang, W. Duan, H. Yao, Y. Wu, S. Fan, H. Zhang, X. Chen, and S. Zhou, Nat. Phys. **12**, 1105 (2016).

[30] L. Huang, T. M. McCormick, M. Ochi, Z. Zhao, M.-t. Suzuki, R. Arita, Y. Wu, D. Mou, H. Cao, J. Yan, N. Trivedi, and A. Kaminski, Nat. Mater. **15**, 1155 (2016).

[31] J. Jiang, Z. K. Liu, Y. Sun, H. F. Yang, R. Rajamathi, Y. P. Qi, L. X. Yang, C. Chen, H. Peng, C.-C. Hwang, S. Z. Sun, S.-K. Mo, I. Vobornik, J. Fujii, S. S. P. Parkin, C. Felser, B. H. Yan, and Y. L. Chen, Nat. Commun. **8**, 13973 (2017).

[32] A. Liang, J. Huang, S. Nie, Y. Ding, Q. Gao, C. Hu, S. He, Y. Zhang, C. Wang, B. Shen, J. Liu, P. Ai, L. Yu, X. Sun, W. Zhao, S. Lv, D. Liu, C. Li, Y. Zhang, Y. Hu *et al.*, arXiv:1604.01706.

[33] N. Xu, Z. J. Wang, A. P. Weber, A. Magrez, P. Bugnon, H. Berger, C. E. Matt, J. Z. Ma, B. B. Fu, B. Q. Lv, N. C. Plumb, M. Radovic, E. Pomjakushina, K. Conder, T. Qian, J. H. Dil, J. Mesot, H. Ding, and M. Shi, arXiv:1604.02116.

[34] S. Borisenko, D. Evtushinsky, Q. Gibson, A. Yaresko, T. Kim, M. N. Ali, B. Buechner, M. Hoesch, and R. J. Cava, arXiv:1507.04847.

[35] G. Chang, S.-Y. Xu, H. Zheng, B. Singh, C.-H. Hsu, I. Belopolski, D. S. Sanchez, G. Bian, N. Alidoust, H. Lin, and M. Z. Hasan, Sci. Rep. **6**, 38839 (2016).

[36] Z. Wang, M. G. Vergniory, S. Kushwaha, M. Hirschberger, E. V. Chulkov, A. Ernst, N. P. Ong, R. J. Cava, and B. A. Bernevig, Phys. Rev. Lett. **117**, 236401 (2016).

[37] J. Kübler and C. Felser, EPL (Europhysics Letters) **114**, 47005 (2016).

[38] H. Yang, Y. Sun, Y. Zhang, W.-J. Shi, S. S. P. Parkin, and B. Yan, New J. Phys. **19**, 015008 (2017).

[39] Y. Zhang, Y. Sun, H. Yang, J. Železný, S. P. P. Parkin, C. Felser, and B. Yan, Phys. Rev. B **95**, 075128 (2017).

[40] M. Hirschberger, S. Kushwaha, Z. Wang, Q. Gibson, S. Liang, C. A. Belvin, B. A. Bernevig, R. J. Cava, and N. P. Ong, Nature Mater. **15**, 1161 (2016).

[41] C. Shekhar, A. K. Nayak, S. Singh, N. Kumar, S.-C. Wu, Y. Zhang, A. C. Komarek, E. Kampert, Y. Skourski, J. Wosnitza, W. Schnelle, A. McCollam, U. Zeitler, J. Kubler, S. S. P. Parkin, B. Yan, and C. Felser, arXiv:1604.01641.

[42] G. Chang, B. Singh, S.-Y. Xu, G. Bian, S.-M. Huang, C.-H. Hsu, I. Belopolski, N. Alidoust, D. S. Sanchez, H. Zheng, H. Lu, X. Zhang, Y. Bian, T.-R. Chang, H.-T. Jeng, A. Bansil, H. Hsu, S. Jia, T. Neupert, H. Lin *et al.*, arXiv:1604.02124.

[43] Y. Kim, B. J. Wieder, C. L. Kane, and A. M. Rappe, Phys. Rev. Lett. **115**, 036806 (2015).

[44] H. Weng, Y. Liang, Q. Xu, R. Yu, Z. Fang, X. Dai, and Y. Kawazoe, Phys. Rev. B **92**, 045108 (2015).

[45] L. S. Xie, L. M. Schoop, E. M. Seibel, Q. D. Gibson, W. Xie, and R. J. Cava, APL Mater. **3**, 083602 (2015).

[46] R. Yu, H. Weng, Z. Fang, X. Dai, and X. Hu, Phys. Rev. Lett. **115**, 036807 (2015).

[47] M. Zeng, C. Fang, G. Chang, Y.-A. Chen, T. Hsieh, A. Bansil, H. Lin, and L. Fu, arXiv:1504.03492.

[48] Q. Xu, Z. Song, S. Nie, H. Weng, Z. Fang, and X. Dai, Phys. Rev. B **92**, 205310 (2015).

[49] H. Huang, S. Zhou, and W. Duan, Phys. Rev. B **94**, 121117 (2016).

[50] G. Bian, T.-R. Chang, R. Sankar, S.-Y. Xu, H. Zheng, T. Neupert, C.-K. Chiu, S.-M. Huang, G. Chang, I. Belopolski, D. S. Sanchez, M. Neupane, N. Alidoust, C. Liu, B. Wang, C.-C. Lee, H.-T. Jeng, C. Zhang, Z. Yuan, S. Jia *et al.*, Nat. Commun. **7**, 10556 (2016).

[51] G. Bian, T.-R. Chang, H. Zheng, S. Velury, S.-Y. Xu, T. Neupert, C.-K. Chiu, S.-M. Huang, D. S. Sanchez, I. Belopolski, N. Alidoust, P.-J. Chen, G. Chang, A. Bansil, H.-T. Jeng, H. Lin, and M. Z. Hasan, Phys. Rev. B **93**, 121113 (2016).

[52] L. M. Schoop, M. N. Ali, C. Straszer, A. Topp, A. Varykhalov, D. Marchenko, V. Duppel, S. S. P. Parkin, B. V. Lotsch, and C. R. Ast, Nat. Commun. **7**, 11696 (2016).

[53] M. Neupane, I. Belopolski, M. M. Hosen, D. S. Sanchez, R. Sankar, M. Szlawska, S.-Y. Xu, K. Dimitri, N. Dhakal, P. Maldonado, P. M. Oppeneer, D. Kaczorowski, F. Chou, M. Z. Hasan, and T. Durakiewicz, Phys. Rev. B **93**, 201104 (2016).

[54] J. Hu, Z. Tang, J. Liu, X. Liu, Y. Zhu, D. Graf, K. Myhro, S. Tran, C. N. Lau, J. Wei, and Z. Mao, Phys. Rev. Lett. **117**, 016602 (2016).

[55] T. Andreas, M. L. Judith, V. Andrei, D. Viola, V. L. Bettina, R. A. Christian, and M. S. Leslie, New J. Phys. **18**, 125014 (2016).

[56] M. M. Hosen, K. Dimitri, I. Belopolski, P. Maldonado, R. Sankar, N. Dhakal, G. Dhakal, T. Cole, P. M. Oppeneer, D. Kaczorowski, F. Chou, M. Z. Hasan, T. Durakiewicz, and M. Neupane, Phys. Rev. B **95**, 161101(R) (2017).

[57] Y. Wu, L.-L. Wang, E. Mun, D. D. Johnson, D. Mou, L. Huang, Y. Lee, S. L. Bud'ko, P. C. Canfield, and A. Kaminski, Nature Phys. **12**, 667 (2016).

[58] J. Hu, Z. Tang, J. Liu, Y. Zhu, J. Wei, and Z. Mao, arXiv:1604.01567.

[59] R. Singha, A. Pariari, B. Satpati, and P. Mandal, Proc. Natl. Acad. Sci. USA **114**, 2468 (2017).

[60] M. N. Ali, L. M. Schoop, C. Garg, J. M. Lippmann, E. Lara, B. Lotsch, and S. Parkin, arXiv:1603.09318.

[61] X. Wang, X. Pan, M. Gao, J. Yu, J. Jiang, J. Zhang, H. Zuo, M. Zhang, Z. Wei, W. Niu, Z. Xia, X. Wan, Y. Chen, F. Song, Y. Xu, B. Wang, G. Wang, and R. Zhang, Adv. Electron. Mater. **2**, 1600228 (2016).

[62] R. Lou, J. Z. Ma, Q. N. Xu, B. B. Fu, L. Y. Kong, Y. G. Shi, P. Richard, H. M. Weng, Z. Fang, S. S. Sun, Q. Wang, H. C. Lei, T. Qian, H. Ding, and S. C. Wang, Phys. Rev. B **93**, 241104 (2016).

[63] D. Takane, Z. Wang, S. Souma, K. Nakayama, C. X. Trang, T. Sato, T. Takahashi, and Y. Ando, Phys. Rev. B **94**, 121108 (2016).

[64] N. Kumar, K. Manna, Y. Qi, S.-C. Wu, L. Wang, B. Yan, C. Felser, and C. Shekhar, Phys. Rev. B **95**, 121109(R) (2017).

[65] C. Chen, X. Xu, J. Jiang, S.-C. Wu, Y. P. Qi, L. X. Yang, M. X. Wang, Y. Sun, N. B. M. Schröter, H. F. Yang, L. M. Schoop, Y. Y. Lv, J. Zhou, Y. B. Chen, S. H. Yao, M. H. Lu, Y. F. Chen, C. Felser, B. H. Yan, Z. K. Liu, and Y. L. Chen, Phys. Rev. B **95**, 125126 (2017).

[66] H. Onken, K. Vierheilig, and H. Hahn, Z. Anorg. Allg. Chem. **333**, 267 (1964).

[67] A. K. Haneveld and F. Jellinek, Recl. Trav. Chim. Pays-Bas **83**, 776 (1964).

[68] I. M. Lifshitz and A. M. Kosevich, JETP **2**, 636 (1956).

[69] D. Shoenberg, *Magnetic Oscillations in Metals* (Cambridge University Press, Cambridge, 1984).

[70] G. P. Mikitik and Y. V. Sharlai, Phys. Rev. Lett. **82**, 2147 (1999).

[71] J. Hu, J. Y. Liu, D. Graf, S. M. A. Radmanesh, D. J. Adams, A. Chuang, Y. Wang, I. Chiorescu, J. Wei, L. Spinu, and Z. Q. Mao, Sci. Rep. **6**, 18674 (2016).

[72] J. Xiong, Y. Luo, Y. H. Khoo, S. Jia, R. J. Cava, and N. P. Ong, Phys. Rev. B **86**, 045314 (2012).

[73] Y. Ando, J. Phys. Soc. Jpn. **82**, 102001 (2013).

[74] M. V. Kartsovnik, Chem. Rev. **104**, 5737 (2004).

[75] S. G. Sharapov, V. P. Gusynin and H. Beck, Phys. Rev. B **69**, 075104 (2004).

[76] J. Xiong, S. K. Kushwaha, T. Liang, J. W. Krizan, M. Hirschberger, W. Wang, R. J. Cava, and N. P. Ong, Science **350**, 413 (2015).

[77] A. B. Pippard, *Magnetoresistance in Metals* (Cambridge University Press, Cambridge, 1989).

[78] R. D. d. Reis, M. O. Ajeesh, N. Kumar, F. Arnold, C. Shekhar, M. Naumann, M. Schmidt, M. Nicklas, and E. Hassinger, New J. Phys. **18**, 085006 (2016).

[79] A. Carrington, Rep. Prog. Phys. **74**, 124507 (2011).

[80] C. Wang and T. Hughbanks, Inorg. Chem. **34**, 5524 (1995).

[81] J. Y. Liu, J. Hu, D. Graf, T. Zou, M. Zhu, Y. Shi, S. Che, S. M. A. Radmanesh, C. N. Lau, L. Spinu, H. B. Cao, X. Ke, and Z. Q. Mao, arXiv:1608.05956.